Comptes Rendus

Géoscience

Sciences de la Planète

Olivier Evrard, Roxanne Durand, Atsushi Nakao, J. Patrick Laceby, Irène Lefèvre, Yoshifumi Wakiyama, Seiji Hayashi, Cécile Asanuma-Brice and Olivier Cerdan

Impact of the 2019 typhoons on sediment source contributions and radiocesium concentrations in rivers draining the Fukushima radioactive plume, Japan

Original Article — External Geophysics, Climate

Impact of the 2019 typhoons on sediment source contributions and radiocesium concentrations in rivers draining the Fukushima radioactive plume, Japan

Olivier Evrard[*, a]**, Roxanne Durand**[a]**, Atsushi Nakao**[b]**, J. Patrick Laceby**[c]**, Irène Lefèvre**[a]**, Yoshifumi Wakiyama**[d]**, Seiji Hayashi**[e]**, Cécile Asanuma-Brice**[f, g]** and Olivier Cerdan**[h]

[a] Laboratoire des Sciences du Climat et de l'Environnement (LSCE/IPSL), Unité Mixte de Recherche 8212 (CEA/CNRS/UVSQ), Université Paris-Saclay, Gif-sur-Yvette, France

[b] Graduate School of Life and Environmental Sciences, Kyoto Prefectural University, Kyoto, Japan

[c] Alberta Environment and Parks (AEP), Calgary, Alberta, Canada

[d] Institute of Environmental Radioactivity (IER), University of Fukushima, Fukushima, Japan

[e] National Institute for Environmental Studies (NIES), Fukushima Branch, Miharu, Japan

[f] CNRS, IFRJ-UMIFRE 19 - MFJ, Tokyo, Japan

[g] Center for Japanese Studies (CRJ-Centre de Recherche sur le Japon), UMR 8173 - EHESS, Paris, France

[h] Bureau de Recherches Géologiques et Minières (BRGM), Orléans, France

E-mails: olivier.evrard@lsce.ipsl.fr (O. Evrard), roxanne.durand094@gmail.com (R. Durand), na_4_ka_triplochiton@kpu.ac.jp (A. Nakao), Patrick.Laceby@gov.ab.ca (J. Patrick Laceby), irene.lefevre@lsce.ipsl.fr (I. Lefèvre), wakiyama@ipc.fukushima-u.ac.jp (Y. Wakiyama), shayashi@nies.go.jp (S. Hayashi), asanuma.brice.cecile@cnrs.jp (C. Asanuma-Brice), o.cerdan@brgm.fr (O. Cerdan)

Abstract. The Fukushima nuclear accident in March 2011 generated a 3000 km^2 plume of soils heavily contaminated with ^{137}Cs. Decontamination was completed early in 2019. Typhoon Hagibis was the first extreme event that occurred in the region after decontamination. Its impact on sediment sources and sediment ^{137}Cs contamination was investigated through the application of a sediment fingerprinting procedure using spectrocolorimetry and geochemical properties. Sediment deposits ($n = 24$) were collected in the Mano and Niida River catchments after the 2019 typhoons, and their signature was compared to that of potential sources (e.g., cropland, forests, and subsurface; $n = 57$). Results demonstrate the dominance of cropland as the main source of sediment (mean: 54%)

---

* Corresponding author.

followed by forests (41%) with much lower contributions of subsurface material (5%). Overall, ^{137}Cs concentrations in sediment were on average 84%–93% lower than the levels recorded after the accident in 2011, which demonstrates the effectiveness of cropland decontamination.

1. Introduction

The Fukushima Daiichi nuclear accident that occurred in March 2011 led to the release of significant quantities of radionuclides, including iodine-131 (^{131}I), cesium-134 (^{134}Cs), and cesium-137 (^{137}Cs), into the atmosphere [Chino et al., 2011]. It is estimated that 20% of the released radionuclides were deposited on the Japanese land surface, forming a plume of approximately 3000 km^2 with initial ^{137}Cs levels greater than 100,000 Bq·m^{-2} northwest of the power plant [Yasunari et al., 2011]. The most problematic radionuclide over the long term is ^{137}Cs as large quantities of this substance were released (12–62 PBq or 10^{15} Bq) [Steinhauser et al., 2014]. Furthermore, its 30-year half-life is significantly longer than that of the other isotopes (8 days for ^{131}I and 2 years for ^{134}Cs). Without remediation measures, it will take approximately two centuries for ^{137}Cs to decay to negligible levels in soils of the main plume.

It is widely accepted that ^{137}Cs is strongly and almost irreversibly bound to particles in continental environments in general [Tamura, 1964] and in soils of Fukushima Prefecture in particular [Nakao et al., 2015]. This radioisotope was shown to be redistributed across landscapes following soil erosion and deposition processes [Evrard et al., 2015]. These transfers are accelerated during flood events [Nagao et al., 2013] including those generated by typhoons, which occur frequently in Japan during the summer and early in autumn [Chartin et al., 2017, Laceby et al., 016a]. The redistribution of ^{137}Cs with sediment during floods is therefore a matter of great concern in this region [Yamashiki et al., 2014].

To accelerate the return of local populations in the fallout-impacted region, Japanese authorities conducted extensive decontamination activities in agricultural and residential areas [Evrard et al., 019c]. These works mainly consisted of the removal of the uppermost 5 cm layer of the soil, which was shown to contain 95%–99% of the ^{137}Cs concentrations [Lepage et al., 2015], and storage in specifically designed areas [Yasutaka et al., 2013]. In contrast, decontamination was not implemented in forest areas covering approximately 75% of the surface area in the main fallout-impacted region [Hashimoto et al., 2012]. This may therefore provide a perennial source of contaminated material to the river systems draining the main radioactive plume [Laceby et al., 016b].

To quantify forest contributions to sediment and sediment-bound ^{137}Cs transported in the rivers draining the main radioactive plume, sediment tracing or fingerprinting techniques that capitalize on the measurement of conservative properties in both potential sources and sediment have been implemented [Haddadchi et al., 2013, Owens et al., 2016, Walling, 2013]. Previous research in the Fukushima region has used different sets of parameters, including ^{137}Cs activity in soils [Evrard et al., 2016], elemental geochemistry [Lepage et al., 2016], organic matter properties [Huon et al., 2018], or even environmental DNA [Evrard et al., 019b]. Recently, the potential of color to discriminate among cropland, forest, and subsurface (e.g., landslide and channel bank collapse) sources of sediment was also demonstrated in these catchments [Evrard et al., 019a]. This method is based on the major contrast observed between the dark-colored Cambisols and Andisols found under croplands and forests compared to the light-colored crushed granite extracted from local quarries. This material is used to replace the ^{137}Cs-contaminated topsoil layer with a new substrate as part of the remediation program.

These techniques were applied before the completion of decontamination works in the main radioactive plume and the progressive reopening of the region to the inhabitants [Asanuma-Brice, 2018]. Early in 2019, soils were progressively prepared to allow for their recultivation through the mixing of the residual initial soil profile with a crushed granite layer (Supplementary Material S1). This process requires the adaptation of the previously developed sediment tracing methods (e.g., based on the color properties) to these new conditions.

Typhoons have been shown to generate extensive soil erosion and river flooding in Japan in general, and the Fukushima region in particular, with the potential to transfer significant quantities of sediment and particle-bound ^{137}Cs in the rivers draining the main radioactive plume [Kurikami et al., 2016, Laceby et al., 016a, Taniguchi et al., 2019]. In October 2019, typhoon no. 19 (Hagibis), which made landfall on Japan on October 12, was reported to have generated the largest number of sediment disaster occurrences (e.g., landslides and mudflows) in Japan since 1982 [Irasawa et al., 2020], killing at least 93 people, including 31 in the Fukushima Prefecture, and leaving 2367 people homeless across Japan [Asanuma-Brice, 2019]. The heavy rainfall recorded during this event also led to the overflow of numerous rivers across Japan, including several coastal rivers draining the main radioactive plume of the Fukushima Prefecture.

As typhoon Hagibis generated extensive soil erosion, landslides, and flooding in the fallout-impacted region, the objective of the current research is to investigate the impact of this heavy rainfall event on sources that delivered sediment to coastal river systems, including decontaminated land, and on sediment ^{137}Cs concentrations. The purpose is to investigate the effectiveness of remediation works and the contribution of forests during this type of extreme event.

2. Materials and methods

2.1. *Study area*

The study was conducted in the Niida (275 km^2) and Mano (175 km^2) coastal catchments (Figure 1) located to the north of the Fukushima Daiichi Nuclear Power Plant (FDNPP) in Fukushima Prefecture, Japan. These catchments include upstream mountainous plateaus located at an altitude of 700–900 m above sea level connected to a coastal plain by deep and strongly incised rivers [Chartin et al., 2017]. The upper plateaus of these catchments were evacuated in 2011 as ^{137}Cs activities in soils ranged from 20 to 75 kBq·kg^{-1}. In contrast, in the coastal plain, the initial ^{137}Cs contamination did not exceed 20 kBq·kg^{-1} [Evrard et al., 2016].

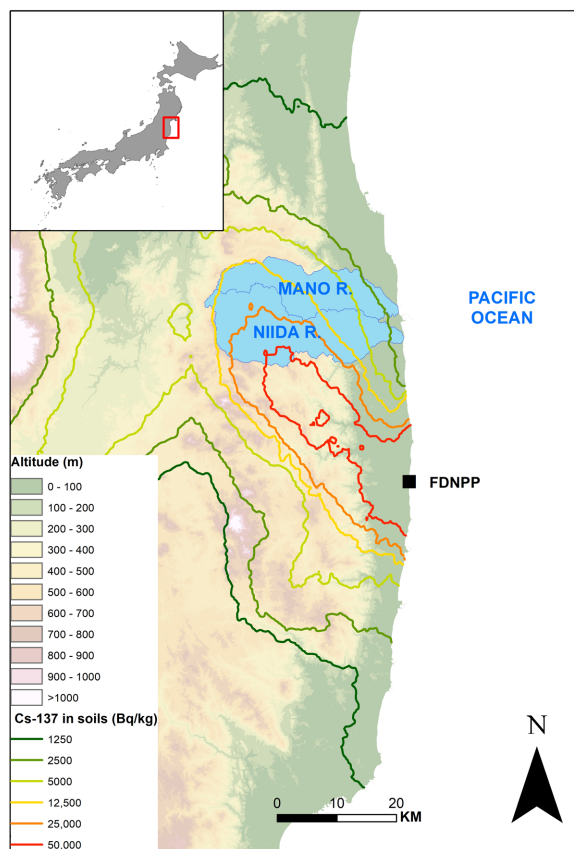Although 75% of the catchment surface in the upper and middle parts of the two catchments is

Figure 1. Location of the Mano and Niida River catchments in northeastern Japan draining a part of the main radioactive plume generated after the FDNPP accident in March 2011. Background initial ^{137}Cs contamination levels from Chartin et al. [2013].

covered with forests, croplands including paddy fields are concentrated along the river network. In the coastal plains, land use is dominated by cropland and residential areas (Figure 2). The Mano and Niida Rivers drain mainly Cambisols and Andisols developed on a granite and granodiorite bedrock in the upper reaches, while Fluvisols overlying sedimentary bedrock are found in the lower catchment reaches and along the river channel [Lepage et al., 2016]. Cambisols are mainly found beneath forests, whereas Andisols are often found beneath forests or croplands [Evrard et al., 019a].

The mean precipitation in the region surrounding the FDNPP is 1420 mm·yr^{-1}. Moreover, 60%
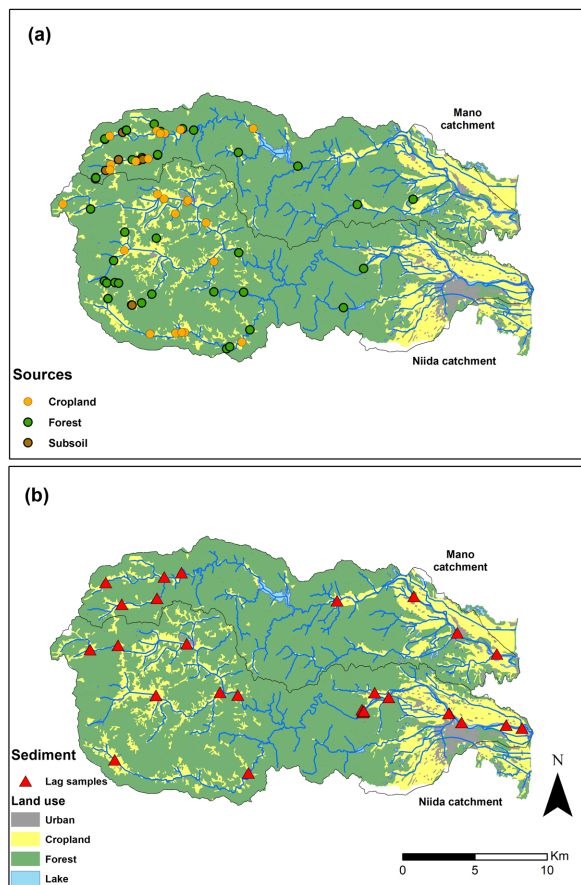
Figure 2. (a) Location of the potential sediment source samples (soil samples) including material from forests, croplands, and subsurfaces collected in Mano and Niida River catchments in 2015 [Laceby et al., 016b] and in March 2019 (this study); (b) location of the sediment lag deposits collected in October 2019 (this study).

of the annual precipitation and 82% of the annual rainfall erosivity occur between June and October, mainly during typhoons and tropical storms [Laceby et al., 016a]. Daily rainfall records from 38 monitoring stations located within a 100 km radius around FDNPP were downloaded from the Japan Meteorological Agency (JMA) website (http://www.jma.go.jp/jma/index.html) to cover the period between the FD-NPP accident in March 2011 and the end of the typhoon season in November 2019.

2.2. *Sample collection and preparation*

Soil samples ($n = 57$), representing potential sources of sediment, were collected in two fieldwork campaigns (Figure 2a). Soils under forest cover ($n = 30$) and subsurface materials ($n = 9$; e.g., channel bank collapse and landslides) were collected in July and August 2015 [Laceby et al., 016b]. In addition, soil samples ready for recultivation ($n = 18$), after plowing and mixing the initial residual soil profile with the uppermost crushed granite layer, were collected in March 2019. These source samples were mainly collected in upper catchment parts, relatively close to the river network, in areas where erosion processes were the most active. Each sample is generated from 10 subsamples collected from the soil surface (upper 2 cm) using a plastic spatula, and it is well mixed and homogenized for analysis.

Sediment lag deposits (mud drapes that settled typically on top of channel-bed sand; $n = 24$) were collected along the main rivers draining the Mano and Niida catchments after the typhoon season on 29 and 30 October 2019 (Figure 2b). At each sampling site, 5 to 10 surface scrapes of deposited sediment, collected along a 5–10 m river reach with a plastic spatula, were composited into one sample.

All soil and sediment samples were dried at 40 °C for 48 h. Then, they were sieved to 63 μm and placed in plastic boxes (15 mL) prior to analyses. All the data including spectrocolorimetric properties, geochemical properties, and radiocesium concentrations are available on the Pangaea data repository (https://doi.org/10.1594/PANGAEA.923582).

2.3. *Spectrocolorimetric analyses*

All soil and sediment samples were analyzed using a portable diffuse reflectance spectrophotometer (Konica Minolta CM-700d) by providing data required to calculate characteristic colorimetric parameters. The spectrophotometer was calibrated before each measurement session by a white and a black gauge. The measurements were performed in triplicate on the plastic boxes in which the samples were stored (15 mL) with a minimum sample quantity of 0.2 g. All measurements were performed with a 3 mm aperture target mask, the standard illuminant D65, and a 10° angle observer, excluding the specular component. The instrument measured

the percentage of spectral reflectance for each of the 39 wavelength classes between 360 and 740 nm at a resolution of 10 nm. The XYZ tristimulus values were calculated on the basis of the color matching functions defined in 1931 by the International Commission on Illumination [CIE, 1931]. These standardized tristimulus values were then transformed into the CIE L*a*b* and CIE L*u*v* Cartesian coordinate systems using the equations given in CIE [1978]. In total, the values of 15 colorimetric parameters were determined for each soil and sediment sample (L*, a*, b*, c*, h, x, y, z, L, a, b, u*, v*, u′, v′).

2.4. *Elemental geochemistry analyses*

All soil and sediment samples were also analyzed using an energy-dispersive X-ray fluorescence spectrometer (ED-XRF; Epsilon 4) to obtain their chemical composition. Measurements were conducted on containers covered with Mylar films with a 10 mm exposure surface. The quantity of material analyzed amounted to a minimum of 0.1 g. Each sample was analyzed thrice to take into account its potential heterogeneity.

The samples were irradiated with a primary beam generated by an X-ray tube. For each measurement, the X-ray tube current and voltage were changed four times according to the four conditions predefined during the calibration carried out specifically for the type of container used for this study (condition ⟨Ni–Mo⟩ with current and voltage set at 50 kV and 0.14 mA; condition ⟨Cr–Co⟩ at 20 kV and 0.14 mA; condition ⟨K–V⟩ at 12 kV and 0.32 mA; condition ⟨F–Si⟩ at 5 kV and 0.7 mA, respectively). The secondary radiation emitted by the irradiated sample was detected, and the software converted the intensities of these rays into elemental concentrations. The samples were determined to contain 19 chemical elements: Mg, Al, Si, K, Ca, Ti, Cr, Mn, Fe, Co, Ni, Cu, Zn, As, Rb, Sr, Zr, Ba, and Pb. As several elements (Cr, As, and Ba) had values below the detection limits for several samples, they were excluded from subsequent analyses.

2.5. *Radiocesium analyses*

The ^{137}Cs activities were determined by gamma spectrometry using low-background coaxial HPGe detectors. Counting times of soil and sediment samples varied between 3×10^4 and 8×10^4 s. The ^{137}Cs activities were measured at the 662 keV emission peak; errors reached approximately 5% at the 95% confidence level. All measured counts were corrected for background levels estimated at least every two months as well as for detector and geometry efficiencies. Results were systematically expressed in Bq·kg^{-1} of dry weight. Counting efficiency and quality assurance were implemented using certified International Atomic Energy Agency reference materials prepared in the same containers as the samples. All radionuclide activities were decay-corrected to the sampling date. The ^{137}Cs activities measured in the lag deposits collected in October 2019 were compared to those measured in the sediment collected at the same location and following the same methodology after spring floods and/or the typhoon season between November 2011 and November 2018 [Chartin et al., 2013, Evrard et al., 2014, 019a, 2016].

2.6. *Sediment source discrimination and apportionment*

The selection of discriminant tracers followed the three-step procedure used for sediment fingerprinting: (i) a range test, where the mean had to be plotted within one standard deviation (SD) of the sources; (ii) the Kruskal–Wallis H test (KW H test); and (iii) a linear discriminant function analysis (DFA) [Wilkinson et al., 2013]. The source contributions were estimated by minimizing the sum of squared residuals of the mass-balance unmixing model. Optimization constraints were set to ensure that source contributions were non-negative and that their sum equaled 1. The unmixing model was solved using source means as model inputs [Tiecher et al., 2019]. Statistical analyses were performed using R software (R Development Core Team, 2017).

3. Results and discussion

3.1. *Rainfall conditions during typhoons in 2019*

Figure 3 presents the distribution of the mean daily rainfall recorded by 38 stations located within a 100 km radius around the FDNPP between 2011 and 2019. During the investigated period, 16 major tropical storms and typhoons generated extensive rainfall (>60 mm) in the study area, representing an average
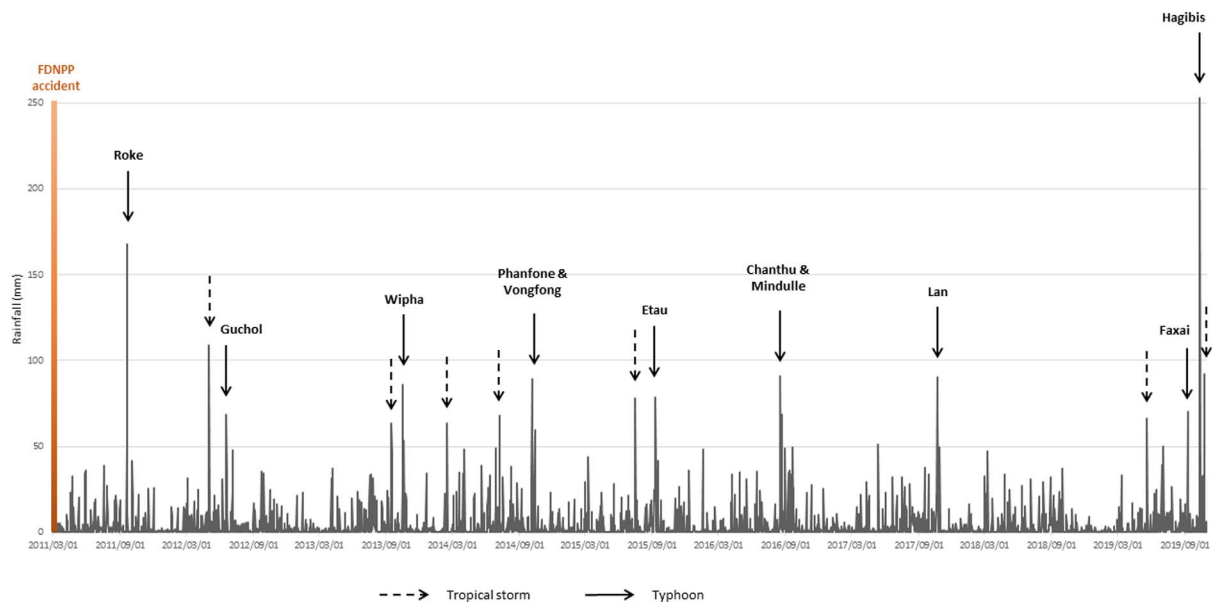
Figure 3. Mean rainfall daily amounts measured at the 38 rainfall monitoring stations surrounding FDNPP from the JMA between March 2011 and November 2019. The main typhoons and tropical storms that affected the region during this period are identified by their names on the graph.

of 1.8 heavy rainfall events occurring each year in the region. All the years between 2011 and 2019 experienced at least one of these heavy events with the exception of 2018. Only two typhoons generated rainfall in the FDNPP region that exceeded 150 mm·d^{-1} after the nuclear accident. The first event (typhoon Roke with a mean rainfall of 168 mm on 21 September 2011; range: 55–268 mm) occurred shortly after the nuclear accident. Typhoon Roke generated extensive flooding and radiocesium export in the rivers draining the main Fukushima radioactive plume [Nagao et al., 2013, Sakuma et al., 2019, Yamashiki et al., 2014].

The second event is typhoon Hagibis, which affected the region on 12 October 2019 (mean rainfall of 253 mm; range: 77–558 mm). Hagibis was clearly the event that generated the highest daily rainfall during the entire rainfall sequence recorded between 2011 and 2019. Furthermore, it took place during a particularly wet autumn season; a mean rainfall of 633 mm was recorded in September and October 2019. This is almost the double of what has been recorded on average during these 2 months in the region between 1977 and 2015 [Laceby et al., 016a]. Accordingly, the antecedent rainfall may have weakened soils and

facilitated the landslides and river flooding that occurred during typhoon Hagibis.

3.2. *Sediment source discrimination and apportionment*

Among the 31 potential fingerprint properties measured and retained for analysis (see Figures in Supplementary Material S2), only four of them were found not to be conservative (Zr, a*, h, u′; Table 1). Following the KW test, only two properties did not provide significant discrimination among the potential sources (Fe, Co; Table 1). From the 25 retained parameters, a suite of 10 properties (L*, Ca, Al, a, z, b, b*, Si, C*, Ti) was selected by the DFA (Table 2). This tracing suite includes six colorimetric properties and four geochemical elements. One of the color parameters (L*) represents the sample brightness [Viscarra Rossel et al., 2006]. Subsurface material containing light-colored granite was logically found to be brighter (mean L* of 58.6) than the other sources (cropland: 46.0; forest: 35.7) developed on Fluvisols, Andisols, and Cambisols (see Supplementary Material S1). The other selected color properties (a, z, b, b*, c*) represent color variations

Table 1. Results of the conservative test and the Kruskal–Wallis test on the suite of potential tracers

		Kruskal–Wallis test		
Property	Conservative	H-value	p-value	Discriminant
Mg	Yes	11.7	<0.01	Yes
Al	Yes	35.6	<0.01	Yes
Si	Yes	27.5	<0.01	Yes
K	No	16.4	<0.01	Yes
Ca	Yes	20.6	<0.01	Yes
Ti	Yes	12.5	<0.01	Yes
Mn	Yes	11.8	<0.01	Yes
Fe	Yes	2.3	0.32	No
Co	Yes	1.0	0.61	No
Ni	Yes	4.8	0.09	No
Cu	Yes	6.1	<0.05	Yes
Zn	Yes	12.9	<0.01	Yes
Rb	Yes	13.1	<0.01	Yes
Sr	Yes	20.4	<0.01	Yes
Zr	No	22.0	<0.01	Yes
Pb	Yes	2.0	0.37	No
L^*	Yes	35.7	<0.01	Yes
a^*	No	16.6	<0.01	Yes
b^*	Yes	27.0	<0.01	Yes
c^*	Yes	25.8	<0.01	Yes
h	No	27.0	<0.01	Yes
x	Yes	18.1	<0.01	Yes
y	Yes	14.2	<0.01	Yes
z	Yes	16.5	<0.01	Yes
L	Yes	35.7	<0.01	Yes
a	Yes	20.2	<0.01	Yes
b	Yes	29.1	<0.01	Yes
u^*	Yes	24.2	<0.01	Yes
v^*	Yes	29.0	<0.01	Yes
u'	No	8.6	<0.05	Yes
v'	Yes	15.6	<0.01	Yes

Table 2. Variables retained by the DFA and associated statistics

Property	Wilks lambda	p-value
L^*	0.30011	<0.01
Ca	0.21889	<0.01
Al	0.17844	<0.01
a	0.14342	<0.01
z	0.09318	<0.01
b	0.08679	<0.01
b^*	0.07259	<0.01
Si	0.06275	<0.01
C^*	0.05784	<0.01
Ti	0.05365	<0.01

Regarding the selected geochemical properties, Al was found to be the most enriched in subsurface material (mean: 110,250 mg·kg^{-1}) compared to other sources with mean values ranging between 65,780 mg·kg^{-1} for forest and 84,730 mg·kg^{-1} for cropland material. This likely reflects the higher levels of gibbsite (aluminum hydroxide) or kaolinite found in subsurface granitic saprolite illuviated from the upper soil depths through soil formation [Nakao et al., 2009]. Ca and Ti are depleted in the subsurface material compared to cultivated and forested land, which is commonly observed in Japanese soils because of leaching and weathering of these elements through the soil profile. In contrast, an enrichment of Si was found in subsurface compared to surface sources [Takeda et al., 2004].

The sediment source contributions calculated by the model (see Supplementary Material S3) show the dominance of cropland (corresponding to the ready-to-cultivate soils) sources in the Mano River catchment (mean: 58%, SD: 29%) followed by forest material (mean: 34%, SD: 18%; Figure 4). In contrast, forest landscapes were the most dominant source in the Niida River catchment (mean: 48%, SD: 22%) followed by cropland (mean: 44%, SD: 30%). In both catchments, subsurface material supplied comparatively low contributions (mean 8–9%) to sediment transiting these coastal river systems.

The relatively high SDs associated with the mean source contributions demonstrate the occurrence of large spatial variations across the two investigated catchments. In the upper catchment area, cropland
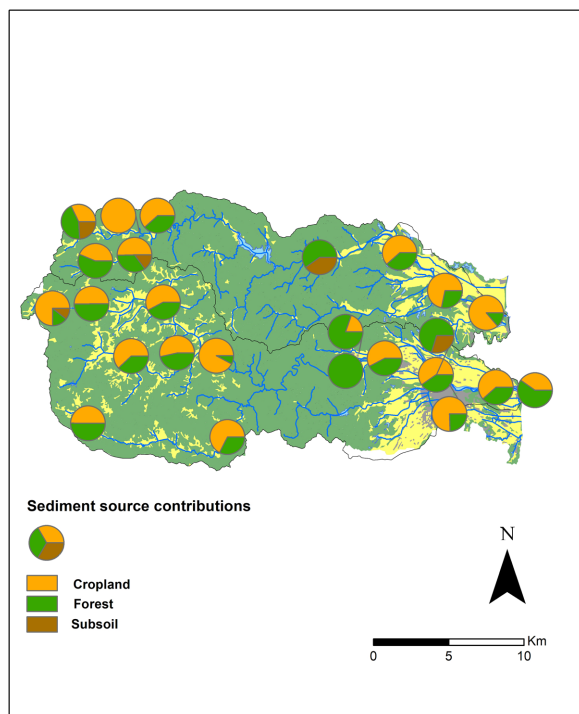
[Viscarra Rossel et al., 2006] with again differences found in subsurface material tending to be more yellow (mean b value: 15.5) than cropland (b: 10.0) and forest (b: 7.0) sources.

Figure 4. Modeled sediment source contributions to sediment collected after the October 2019 typhoons in the Niida and Mano River catchments.

was the main sediment source in both the Niida (mean: 57%, SD: 20%) and the Mano River watersheds (mean: 60%, SD: 25%). Significant forest and subsurface contributions were found locally (Figure 4), mainly in the central part of the Mano River catchment (forest: 60%; subsurface: 40%). In the central part of the Niida River catchment, sediment samples were even modeled to originate exclusively from forest sources. This is likely explained by the incision of the river in steep woodland areas in this area. Finally, in the coastal plain, the model calculated that a mix of forest (mean: 51%, SD: 23%), cropland (mean: 31%, SD: 34%), and subsurface (mean: 18%, SD: 24%) sources delivered sediment, which is consistent with the results obtained in upstream sections.

The results from the current research contrast with those obtained in previous studies conducted in the same study areas. Evrard et al. [019a] used color properties to discriminate among cropland, forest, and subsurface source contributions to sediment

collected after major typhoons and spring floods in the same catchments between 2011 and 2017. Although they also found a dominant contribution of cropland (mean: 56%, SD: 34%), subsoil (mean: 26%, SD: 16%) and forests (mean: 21%, SD: 24%) were also reported to provide significant sources of material to the river systems. Similar results were obtained by Laceby et al. [016b], who used organic matter properties to differentiate the sources of sediment delivered to these river systems between 2012 and 2014. They found that the dominant contribution of subsurface sources (mean: 45%, SD: 26%) exceeded those of cropland (mean: 38%, SD: 19%) and forest sources (mean: 17%, SD: 10%). Huon et al. [2018] followed a similar approach on sediment cores collected in the Mano Dam reservoir. They also calculated significant sediment contributions from subsurface (mean: 25%, SD: 4%) and forests (mean: 27%, SD: 6%) despite cropland being quantified to provide the dominant sediment supply to the reservoir (mean: 48%, SD: 7%).

The much lower subsurface contributions (mean: 5%, SD: 11%) found in the current research compared to those quantified in previous studies are likely explained by the fact that landslides occurred after the flood peak and mobilized relatively coarser material that deposited at the foot of hillslopes or in the major floodplain (Supplementary Material S4). However, this material stored in the vicinity of the river channel will likely be preferentially remobilized during subsequent flood events. The large dominance of cropland material (mean: 54%, SD: 26%) is likely explained by the low vegetation cover available on most fields that had just been prepared for recultivation (see Supplementary Material S1) as well as by its direct connectivity to the river channel [Chartin et al., 2013] mainly during heavy typhoons such as Hagibis [Chartin et al., 2017].

3.3. *Radiocesium concentrations in river sediment*

The ^{137}Cs activities measured in lag deposits were slightly higher in sediment collected in the Niida River (mean: 2385 Bq·kg^{-1}; SD: 2006 Bq·kg^{-1}; Figure 5) compared to the Mano River (mean: 1877 Bq·kg^{-1}; SD: 1818 Bq·kg^{-1}; Figure 5), which is likely explained by the fact that the first river drains initially more contaminated soils (Figure 1).
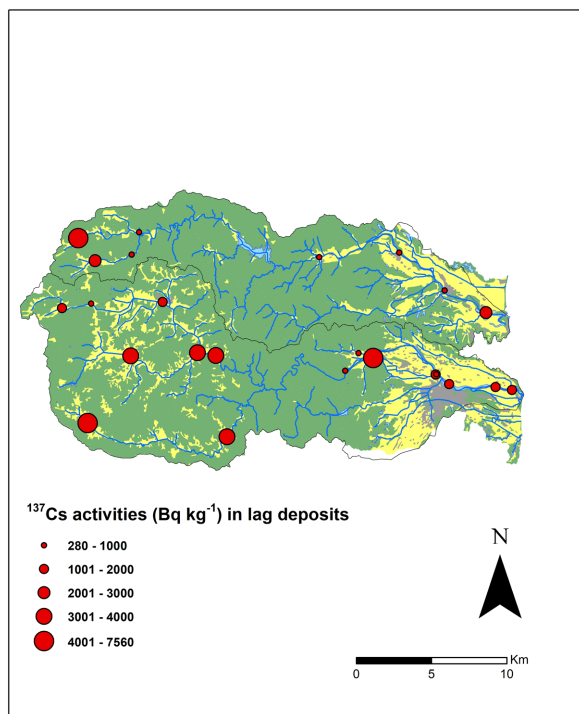
Figure 5. Concentrations of ^{137}Cs measured in sediment samples collected after the October 2019 typhoons in the Mano and Niida River catchments.

Overall, the extensive soil erosion processes that occurred in the investigated catchments during the 2019 typhoons did not lead to an increase in the ^{137}Cs contamination levels in sediment transiting these coastal river systems compared to the previous sampling campaigns. The current research demonstrates that the decrease in ^{137}Cs activities measured in sediment collected between 2011 and 2015 at the same locations [Chartin et al., 2017] continued between 2016 and 2019. Compared to the mean levels observed in sediment collected in 2011, this decrease in ^{137}Cs concentrations reached 93% in the Niida River (2385 Bq·kg^{-1} compared to 34,100 Bq·kg^{-1}) and 84% in the Mano River (1877 Bq·kg^{-1} in 2019 compared to 11,900 Bq·kg^{-1} in 2011). This is likely explained by the dominance of the decontaminated cropland soil contributions found in these lag deposits and demonstrated by the sediment fingerprinting approach conducted in the current research. The slightly higher ^{137}Cs levels measured in sediment samples collected in the coastal reaches of the Niida

River (mean: 2442 Bq·kg^{-1}; maximum: 7559 Bq·kg^{-1}) remained below the 8000 Bq·kg^{-1} threshold for contaminated material being disposed of in conventional landfills [Evrard et al., 019c] or close to or below the threshold for material being used to build road embankments [Takai et al., 2018].

3.4. *Perspectives for regional recovery in Fukushima and for future research*

Overall, the results obtained in the current research showed that the heavy rainfall observed during typhoons in 2019 did not lead to a renewed increase in ^{137}Cs activity levels in sediment transiting the Mano and Niida Rivers. Furthermore, our research demonstrated that these concentrations continued to decrease as documented in rivers draining the main Fukushima radioactive plume since 2011 [Sakuma et al., 2019, Taniguchi et al., 2019, Yoshimura et al., 2015]. The dominant contribution of soils ready for recultivation, providing the main sediment supply in the region, was likely driven by the extensive plowing operations conducted in 2019 and the fact that the plowed soils remained temporarily uncovered by vegetation during the 2019 rainy season. This may change in the future as local farmers receive incentives from the local authorities to restart agricultural production (e.g., cultivation of flowers, buckwheat, and feed rice) in the area. This will provide a denser cover of the soil by vegetation throughout the year and protect it from erosion. However, the plowing of the residual initial soil profile with the crushed granite layer raises several questions regarding the fertility of these soils and the use of K fertilizers to limit the transfer of the residual ^{137}Cs to plants [Kurokawa et al., 2019].

The results obtained in the current research for the Mano and Niida River catchments may not necessarily be extended to all the rivers draining the main radioactive pollution plume in Fukushima Prefecture as sediment source contributions depend on local land use and the progress of remediation works at each site. Furthermore, the delineation of restricted access areas and associated rules were modified by recent political decisions. For instance, on 26 August 2020, the Japanese Government lifted the evacuation order in the areas located in the vicinity of the FD-NPP despite the absence of remediation in this zone. However, it may be anticipated that few inhabitants

will return without the implementation of decontamination.

The role of forests as a potential perennial supply of sediment and associated ^{137}Cs to river systems in this region in general, and in the more densely inhabited coastal areas in particular, remains one of the main challenges for investigation in the future. After complex processes of transfer and migration of ^{137}Cs from the canopy, the tree trunk, and the litter to mineral horizons of soils beneath woodlands [Hashimoto et al., 2020], forests may continue supplying contaminated material to rivers and ultimately to the Pacific Ocean, where ^{137}Cs may desorb [Takata et al., 2020] and it may incorporate marine biota or seafloor sediment [Buesseler, 2020]. Accordingly, the reduction in potential downstream transfers of ^{137}Cs from forested regions through remediation and/or ongoing ^{137}Cs management will likely be an important priority for local inhabitants [Koarashi et al., 2020].

4. Conclusions

The typhoons that occurred in September and October 2019, including typhoon Hagibis, triggered extensive erosion and landslides across Japan and the Fukushima-impacted region. They generated widespread river flooding, including in the catchments draining the main radioactive plume. Typhoon Hagibis was the strongest storm recorded since 2011, and it was the first extreme event that occurred after the completion of decontamination works in agricultural and residential areas. A suite of 10 geochemical and spectrocolorimetric properties with a strong physicochemical basis for source discrimination was selected to quantify the origin of the material transported in the river systems during this event.

The results obtained using the sediment tracing approach developed in the current research demonstrated that sediment mainly originated from decontaminated soils ready for recultivation and forest material, with very limited subsoil contributions, which differs from the results obtained in previous studies. This finding underlines the need to quantify sediment source contributions after contrasted events as the dominant sources may change depending on the intensity of rainfall events or the magnitude of anthropogenic disturbances (e.g., decontamination). These results will be particularly helpful to improve our understanding of the main factors controlling the soil erosion response of these landscapes, which is a prerequisite for designing an effective soil erosion model simulating sediment and contaminant fluxes in this region. The current research also demonstrated that the typhoon did not lead to an increase in ^{137}Cs contamination levels recorded in sediment that transited these river systems compared to those recorded during previous years. Furthermore, ^{137}Cs concentrations remained systematically below the thresholds allowed for material to be disposed of in conventional landfills.

In the future, the impact of land recultivation and the perennial contribution of forests to sediment and associated ^{137}Cs delivered to these river systems should continue to be investigated to improve our understanding of the consequences of extreme events and human disturbances on sediment and contaminant transfers in river networks. The long-term impact of forest landslides, which leads to massive sediment deposition on footslopes, should also be monitored along with the development of remediation strategies in woodland ecosystems, which cover approximately 75% of the landscapes in this region.

Supplementary data

Supporting information for this article is available on the journal's website under https://doi.org/10.5802/crgeos.42 or from the author.

References

Asanuma-Brice, C. (2018). Fukushima, l'impossible retour dans les villages de l'ancienne zone

d'évacuation: l'exemple d'Iitate (In French); http://geoconfluences.ens-lyon.fr/actualites/ eclairage/fukushuma-iitate-impossible-retour. Géoconfluences.

Asanuma-Brice, C. (2019). Les catastrophes naturelles ressuscitent le désastre nucléaire (In French). http://japosphere.blogs.liberation. fr/2019/11/25/les-catastrophes-naturelles-ressuscitent-le-desastre-nucleaire/ (latest access on 31 August 2020).

Buesseler, K. O. (2020). Opening the floodgates at Fukushima. *Science*, 369:621–622.

Chartin, C., Evrard, O., Laceby, J. P., Onda, Y., Ottlé, C., Lefèvre, I., and Cerdan, O. (2017). The impact of typhoons on sediment connectivity: lessons learnt from contaminated coastal catchments of the Fukushima Prefecture (Japan). *Earth Surf. Process. Landf.*, 42:306–317.

Chartin, C., Evrard, O., Onda, Y., Patin, J., Lefèvre, I., Ottlé, C., Ayrault, S., Lepage, H., and Bonté, P. (2013). Tracking the early dispersion of contaminated sediment along rivers draining the Fkushima radioactive pollution plume. *Anthropocene*, 1:23–34.

Chino, M., Nakayama, H., Nagai, H., Terada, H., Katata, G., and Yamazawa, H. (2011). Preliminary estimation of release amounts of ^{131}I and ^{137}Cs accidentally discharged from the Fukushima Daiichi nuclear power plant into the atmosphere. *J. Nucl. Sci. Technol.*, 48:1129–1134.

CIE, C. (1978). Publication No. 15, Supplement Number 2 (E-1.3.1, 1971): Official Recommendations on Uniform Color Spaces, Color-Difference Equations, and Metric Color Terms. Commission Internationale de L'Eclairage.

CIE, C. U. P. C. (1931). Commission internationale de L'Eclairage Proceedings.

Evrard, O., Chartin, C., Onda, Y., Lepage, H., Cerdan, O., Lefevre, I., and Ayrault, S. (2014). Renewed soil erosion and remobilisation of radioactive sediment in Fukushima coastal rivers after the 2013 typhoons. *Sci. Rep.*, 4.

Evrard, O., Durand, R., Foucher, A., Tiecher, T., Sellier, V., Onda, Y., Lefèvre, I., Cerdan, O., and Laceby, J. P. (2019a). Using spectrocolourimetry to trace sediment source dynamics in coastal catchments draining the main Fukushima radioactive pollution plume (2011–2017). *J. Soils Sedim.*, 19:3290–3301.

Evrard, O., Laceby, J. P., Ficetola, G. F., Gielly, L., Huon, S., Lefevre, I., Onda, Y., and Poulenard, J. (2019b). Environmental DNA provides information on sediment sources: a study in catchments affected by Fukushima radioactive fallout. *Sci. Total Environ.*, 665:873–881.

Evrard, O., Laceby, J. P., Lepage, H., Onda, Y., Cerdan, O., and Ayrault, S. (2015). Radiocesium transfer from hillslopes to the Pacific Ocean after the Fukushima Nuclear Power Plant accident: a review. *J. Environ. Radioact.*, 148:92–110.

Evrard, O., Laceby, J. P., and Nakao, A. (2019c). Effectiveness of landscape decontamination following the Fukushima nuclear accident: a review. *Soil*, 5:333–350.

Evrard, O., Laceby, J. P., Onda, Y., Wakiyama, Y., Jaegler, H., and Lefevre, I. (2016). Quantifying the dilution of the radiocesium contamination in Fukushima coastal river sediment (2011–2015). *Sci. Rep.*, 6.

Haddadchi, A., Ryder, D. S., Evrard, O., and Olley, J. (2013). Sediment fingerprinting in fluvial systems: review of tracers, sediment sources and mixing models. *Internat. J. Sediment. Res.*, 28:560–578.

Hashimoto, S., Imamura, N., Kaneko, S., Komatsu, M., Matsuura, T., Nishina, K., and Ohashi, S. (2020). New predictions of ^{137}Cs dynamics in forests after the Fukushima nuclear accident. *Sci. Rep.*, 10.

Hashimoto, S., Ugawa, S., Nanko, K., and Shichi, K. (2012). The total amounts of radioactively contaminated materials in forests in Fukushima, Japan. *Sci. Rep.*, 2.

Huon, S., Hayashi, S., Laceby, J. P., Tsuji, H., Onda, Y., and Evrard, O. (2018). Source dynamics of radiocesium-contaminated particulate matter deposited in an agricultural water reservoir after the Fukushima nuclear accident. *Sci. Total Environ.*, 61:1079–1090.

Irasawa, M., Koi, T., Tsou, C.-Y., Kato, N., Matsuo, S., Arai, M., Kaibori, M., Yamada, T., Kasai, M., and Wakahara, T. (2020). October 2019 Sediment disaster in the Tohoku region owing to typhoon no. 19 (Tyhpoon Hagibis). *Internat. J. Erosion Control Eng.*, 13:48–55.

Koarashi, J., Atarashi-Andoh, M., Nishimura, S., and Muto, K. (2020). Effectiveness of decontamination by litter removal in Japanese forest ecosystems affected by the Fukushima nuclear accident. *Sci. Rep.*, 10.

Kurikami, H., Funaki, H., Malins, A., Kitamura, A., and Onishi, Y. (2016). Numerical study of sediment and ¹³⁷Cs discharge out of reservoirs during various scale rainfall events. *J. Environ. Radioact.*, 164:73–83.

Kurokawa, K., Nakao, A., Tsukada, H., Mampuku, Y., and Yanai, J. (2019). Exchangeability of ¹³⁷Cs and K in soils of agricultural fields after decontamination in the eastern coastal area of Fukushima. *Soil Sci. Plant Nutrition*, 65(4):401–408.

Laceby, J. P., Chartin, C., Evrard, O., Onda, Y., Garcia-Sanchez, L., and Cerdan, O. (2016a). Rainfall erosivity in catchments contaminated with fallout from the Fukushima Daiichi nuclear power plant accident. *Hydrol. Earth Syst. Sci.*, 20:2467–2482.

Laceby, J. P., Huon, S., Onda, Y., Vaury, V., and Evrard, O. (2016b). Do forests represent a long-term source of contaminated particulate matter in the Fukushima Prefecture? *J. Environ. Manage.*, 183:742–753.

Lepage, H., Evrard, O., Onda, Y., Lefevre, I., Laceby, J. P., and Ayrault, S. (2015). Depth distribution of cesium-137 in paddy fields across the Fukushima pollution plume in 2013. *J. Environ. Radioact.*, 147:157–164.

Lepage, H., Laceby, J. P., Bonté, P., Joron, J.-L., Onda, Y., Lefèvre, I., Ayrault, S., and Evrard, O. (2016). Investigating the source of radiocesium contaminated sediment in two Fukushima coastal catchments with sediment tracing techniques. *Anthropocene*, 13:57–68.

Nagao, S., Kanamori, M., Ochiai, S., Tomihara, S., Fukushi, K., and Yamamoto, M. (2013). Export of ¹³⁴Cs and ¹³⁷Cs in the Fukushima river systems at heavy rains by typhoon Roke in September 2011. *Biogeosciences*, 10:6215–6223.

Nakao, A., Funakawa, S., Watanabe, T., and Kosaki, T. (2009). Pedogenic alterations of illitic minerals represented by radiocaesium interception potential in soils with different soil moisture regimes in humid Asia. *Eur. J. Soil Sci.*, 60:139–152.

Nakao, A., Takeda, A., Ogasawara, S., Yanai, J., Sano, O., and Ito, T. (2015). Relationships between paddy soil radiocesium interception potentials and physicochemical properties in Fukushima, Japan. *J. Environ. Qual.*, 44:780–788.

Owens, P. N., Blake, W. H., Gaspar, L., Gateuille, D., Koiter, A. J., Lobb, D. A., Petticrew, E. L., Reiffarth, D. G., Smith, H. G., and Woodward, J. C. (2016). Fingerprinting and tracing the sources of soils and sediments: earth and ocean science, geoarchaeological, forensic, and human health applications. *Earth Sci. Rev.*, 162:1–23.

Sakuma, K., Nakanishi, T., Yoshimura, K., Kurikami, H., Nanba, K., and Zheleznyak, M. (2019). A modeling approach to estimate the ¹³⁷Cs discharge in rivers from immediately after the Fukushima accident until 2017. *J. Environ. Radioact.*, 208–209.

Steinhauser, G., Brandl, A., and Johnson, T. E. (2014). Comparison of the Chernobyl and Fukushima nuclear accidents: a review of the environmental impacts. *Sci. Total Environ.*, 470–471:800–817.

Takai, S., Sawaguchi, T., and Takeda, S. (2018). Dose estimation in recycling of decontamination soil resulting from the Fukushima NPS accident for road embankments. *Health Phys.*, 115:439–447.

Takata, H., Aono, T., Aoyama, M., Inoue, M., Kaeriyama, H., Suzuki, S., Tsuruta, T., Wada, T., and Wakiyama, Y. (2020). Suspended particle-water interactions increase dissolved ¹³⁷Cs activities in the nearshore seawater during typhoon Hagibis. *Environ. Sci. Technol.*, 54(17):10678–10687.

Takeda, A., Kimura, K., and Yamasaki, S.-i. (2004). Analysis of 57 elements in Japanese soils, with special reference to soil group and agricultural use. *Geoderma*, 119:291–307.

Tamura, T. (1964). Consequences of activity release: selective sorption reactions of cesium with soil minerals. *Nucl. Safety*, 5:262–268.

Taniguchi, K., Onda, Y., Smith, H. G., Blake, W., Yoshimura, K., Yamashiki, Y., Kuramoto, T., and Saito, K. (2019). Transport and redistribution of radiocesium in Fukushima fallout through rivers. *Environ. Sci. Technol.*, 53:12339–12347.

Tiecher, T., Ramon, R., Laceby, J. P., Evrard, O., and Minella, J. P. G. (2019). Potential of phosphorus fractions to trace sediment sources in a rural catchment of southern Brazil: comparison with the conventional approach based on elemental geochemistry. *Geoderma*, 337:1067–1076.

Viscarra Rossel, R. A., Minasny, B., Roudier, P., and McBratney, A. B. (2006). Colour space models for soil science. *Geoderma*, 133:320–337.

Walling, D. E. (2013). The evolution of sediment source fingerprinting investigations in fluvial systems. *J. Soils Sedim.*, 13:1658–1675.

Wilkinson, S., Hancock, G., Bartley, R., Hawdon, A., and Keen, R. (2013). Using sediment tracing to

assess processes and spatial patterns of erosion in grazed rangelands, Burdekin River basin, Australia. *Agric. Ecosyst. Environ.*, 180:90–102.

Yamashiki, Y., Onda, Y., Smith, H. G., Blake, W. H., Wakahara, T., Igarashi, Y., Matsuura, Y., and Yoshimura, K. (2014). Initial flux of sediment-associated radiocesium to the ocean from the largest river impacted by Fukushima Daiichi Nuclear Power Plant. *Sci. Rep.*, 4.

Yasunari, T. J., Stohl, A., Hayano, R. S., Burkhart, J. F., Eckhardt, S., and Yasunari, T. (2011). Cesium-137 deposition and contamination of Japanese soils due to the Fukushima nuclear accident. *Proc. Natl Acad. Sci. USA*, 108:19530–19534.

Yasutaka, T., Naito, W., and Nakanishi, J. (2013). Cost and effectiveness of decontamination strategies in radiation contaminated areas in Fukushima in regard to external radiation dose. *PLoS One*, 8.

Yoshimura, K., Onda, Y., Sakaguchi, A., Yamamoto, M., and Matsuura, Y. (2015). An extensive study of the concentrations of particulate/dissolved radiocaesium derived from the Fukushima Dai-ichi Nuclear Power Plant accident in various river systems and their relationship with catchment inventory. *J. Environ. Radioact.*, 139:370–378.